Acta Biotheor
DOI 10.1007/s10441-015-9271-y

REGULAR ARTICLE

Population Density and Moment-based Approaches to Modeling Domain Calcium-mediated Inactivation of L-type Calcium Channels

Xiao Wang[1] · **Kiah Hardcastle**[1] · **Seth H. Weinberg**[1] · **Gregory D. Smith**[1]

Received: 3 April 2015 / Accepted: 16 September 2015

Abstract We present a population density and moment-based description of the stochastic dynamics of domain Ca^{2+}-mediated inactivation of L-type Ca^{2+} channels. Our approach accounts for the effect of heterogeneity of local Ca^{2+} signals on whole cell Ca^{2+} currents; however, in contrast with prior work, e.g., Sherman et al. (Biophys J 58(4):985–995, 1990), we do not assume that Ca^{2+} domain formation and collapse are fast compared to channel gating. We demonstrate the population density and moment-based modeling approaches using a 12-state Markov chain model of an L-type Ca^{2+} channel introduced by Greenstein and Winslow (Biophys J 83(6):2918–2945, 2002). Simulated whole cell voltage clamp responses yield an inactivation function for the whole cell Ca^{2+} current that agrees with the traditional approach when domain dynamics are fast. We analyze the voltage-dependence of Ca^{2+} inactivation that may occur via slow heterogeneous domain $[Ca^{2+}]$. Next, we find that when channel permeability is held constant, Ca^{2+}-mediated inactivation of L-type channels increases as the domain time constant increases, because a slow domain collapse rate leads to increased mean domain $[Ca^{2+}]$ near open channels; conversely, when the maximum domain $[Ca^{2+}]$ is held constant, inactivation decreases as the domain time constant increases. Comparison of simulation results using population densities and moment equations confirms the computational efficiency of the moment-based approach, and enables the validation of two distinct methods of truncating and closing the open system of moment equations. In general, a slow domain time constant requires higher order moment truncation for agreement between moment-based and population density simulations.

✉ Gregory D. Smith
greg@as.wm.edu

[1] Department of Applied Science, The College of William & Mary, McGlothlin-Street Hall, Rm 305, Williamsburg, VA 23187, USA

Keywords L-type Ca^{2+} channel · Population density model · Moment-based model · Ca^{2+}-dependent inactivation

1 Introduction

Voltage-gated Ca^{2+} channels fall into three main groups: Ca_v1 (L-type, L for "long lasting"), Ca_v2 (P-, N-, and R-type), and Ca_v3 (T-type, T for "transient") (Lipscombe et al. 2002). Among them, plasma membrane L-type Ca^{2+} channels (LCCs) are widely expressed in many tissues and are known to play an important role in Ca^{2+}-dependent responses of electrically excitable cells. In cardiac myocytes, for example, Ca^{2+} influx via L-type Ca^{2+} channels into the dyadic subspace triggers sarcoplasmic reticulum (SR) Ca^{2+} release and muscle cell contraction (Bers 2002; Cheng et al. 1993; Cannell et al. 1995). L-type Ca^{2+} channels also play a key role in coupling synaptic excitation to activation of transcriptional events that contribute to neuronal plasticity (Murphy et al. 1991). The activation of LCCs is voltage-dependent while the inactivation occurs via both voltage- and Ca^{2+}-dependent mechanisms; consequently, the formation of Ca^{2+} microdomains following LCC influx can greatly influence the stochastic gating of LCCs and the physiology of excitable cells (Haack and Rosenberg 1994; Budde et al. 2002).

There are four subtypes of LCCs that are denoted $Ca_v1.1$–1.4. $Ca_v1.1$ is primarily found in skeletal muscle and $Ca_v1.4$ is mainly found in retinal cells (Lipscombe et al. 2004; Baumann et al. 2004). $Ca_v1.2$ and 1.3 are highly expressed in cardiac myocytes and cells of the central nervous system (Ertel et al. 2000; Simon et al. 2003). In neuroendocrine cells, $Ca_v1.2$ and 1.3 are both involved in action potential generation, bursting activity and hormone secretion (Lipscombe et al. 2004; Marcantoni et al. 2007). $Ca_v1.3$ is biophysically and pharmacologically distinct from $Ca_v1.2$. For example, $Ca_v1.3$ activates at a more hyperpolarized voltage, has faster activation, and slower and less complete voltage-dependent inactivation than $Ca_v1.2$ (Koschak et al. 2001; Vandael et al. 2010). In the heart, $Ca_v1.2$-mediated Ca^{2+} currents play an important role in systolic events such as excitation-contraction (EC) coupling (the triggered release of SR Ca^{2+}) (Huang et al. 2014) and the plateau depolarization (phase 2) of the action potential (Christel and Lee 2012). $Ca_v1.3$, on the other hand, is highly expressed in cardiac pacemaker cells and is the major regulator of ryanodine receptor-dependent (RyR-dependent) local Ca^{2+} release during the diastolic phase (Torrente et al. 2011). Inactivation of $Ca_v1.2$ channels is both voltage- and Ca^{2+}-dependent (Budde et al. 2002); however, certain $Ca_v1.4$ L-type channels do not exhibit Ca^{2+}-dependent inactivation (Lipscombe et al. 2004). L-type Ca^{2+} channels that undergo Ca^{2+}-dependent inactivation do not in fact result in long lasting currents, in spite of the traditional nomenclature (Lipscombe et al. 2004).

Models of Ca^{2+} inactivation often assume a high density of Ca^{2+} channels and the slow accumulation of intracellular Ca^{2+} in a cortical shell near the plasma membrane (Li et al. 1995). In the context of low density Ca^{2+} channels, it may be assumed that spatially localized high [Ca^{2+}] regions (Ca^{2+} domains) form near any individual channel when that particular channel is open (Fig. 1, left panel). In both shell and domain models, it is usually assumed that stochastic gating of L-type channels and the dynamics of the associated domains are independent except through global coupling via the bulk [Ca^{2+}] and plasma membrane voltage (Zweifach and Lewis 1995). For example, the domain model proposed and investigated by Sherman et al. (1990) took this form and further assumed that Ca^{2+} domains form instantaneously when a channel activates, and collapse instantaneously when a channel de-activates or inactivates. This rapid-equilibrium formulation of domain Ca^{2+}-mediated inactivation of L-type Ca^{2+} channels is viable and often utilized as an alternative to shell models. Nevertheless, when the dynamics of Ca^{2+} channel activation and inactivation are not slow compared to domain formation and collapse, the assumption of rapidly equilibrating domain [Ca^{2+}] might be inadequate.

In recent years, computational models of cardiac myocytes have been developed to account for local control of Ca^{2+}-induced Ca^{2+} release and heterogeneous dyadic subspace and junctional SR [Ca^{2+}] (Greenstein and Winslow 2002; Tanskanen et al. 2005; Hartman et al. 2010; Williams et al. 2011). In these models, a large number of Ca^{2+} release units (CaRUs) are simulated, each of which is represented by a discrete-state continuous time Markov chain and associated dyadic subspace and junctional SR compartment. Unfortunately, when the description of CaRU gating

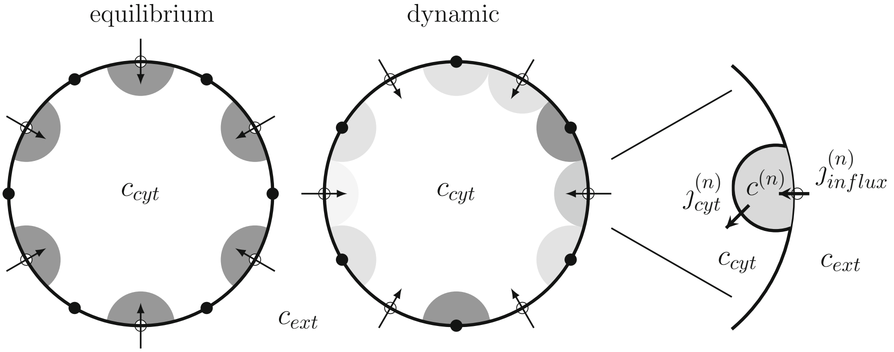

Fig. 1 Comparison of equilibrium and dynamic domain models for Ca^{2+}-mediated inactivation of L-type Ca^{2+} channels. In equilibrium domain models, low density channels are not only locally controlled, but also inactivated by a domain [Ca^{2+}] that is slaved to the channel state (high concentration when *open* and low concentration when *closed*). The *open* and *closed* channels are represented by *arrows* with *open* and *filled circles*, respectively. In the dynamic domain model presented here, low density channels experience heterogeneous domain [Ca^{2+}] that depends on channel state in a more realistic and time-dependent manner. The *right panel* shows the fluxes associated with a minimal formulation of a single domain. Extracellular, cytosolic, and domain [Ca^{2+}] are denoted by c_{ext}, c_{cyt}, and $c^{(n)}$, respectively. The domain influx rate ($J^{(n)}_{influx}$) is nonzero when the Ca^{2+} channel in the *nth* domain is *open*. The diffusion-mediated flux of the *nth* domain Ca^{2+} to the cytosol is denoted by $J^{(n)}_{cyt}$

includes many channel states, the runtime of the Markov chain modeling approach can be excessive.

To avoid the computationally demanding task of performing Monte Carlo simulations of a large number of CaRUs, Williams et al. (2007) presented an approach to modeling local control and EC coupling in cardiac myocytes that uses probability densities to represent heterogeneous time-dependent local Ca^{2+} signals in a large number of dyadic subspaces and junctional SR domains. Population density approaches are an alternative to Monte Carlo simulations that produce realistic and computationally efficient models by using a master equation to represent heterogeneous local Ca^{2+} signals in dyadic subspaces and junctional SR domains (Williams et al. 2007). This approach involves the numerical solution of advection-reaction equations for the time-dependent bivariate probability density of subspace and junctional SR $[Ca^{2+}]$ conditioned on CaRU state, coupled to ordinary differential equations (ODEs) for the bulk myoplasmic and network SR $[Ca^{2+}]$.

Moreover, an associated moment-based approach to simulating the probability distribution of junctional SR $[Ca^{2+}]$ was developed and was benchmarked to be several orders of magnitude faster than conventional Monte Carlo simulation of the dynamics of local Ca^{2+} associated with a physiological number of CaRUs (Williams et al. 2008). The moment-based method begins with the derivation of a system of ODEs describing the time-evolution of the moments of the univariate probability density functions for junctional SR $[Ca^{2+}]$ jointly distributed with CaRU state. This open system of ODEs is then closed using an algebraic relationship that expresses the third moment of junctional SR $[Ca^{2+}]$ as a function of the first and second moments.

In this paper, we use the technique of population density and moment-based modeling (Williams et al. 2007, 2008) to extend the framework for domain Ca^{2+}-mediated inactivation of LCCs in a manner that does not assume a rapidly equilibrating domain, and accounts for time-dependent dynamics of domain formation and collapse (Fig. 1, middle panel). We validate this modeling approach by comparison to the Markov chain stochastic simulation algorithm (SSA) (Gillespie 1976) and investigate the dependence of the inactivation function on the exponential time constant of domain collapse.

The remainder of this paper is organized as follows. First, we formulate a population density approach to modeling domain Ca^{2+}-mediated inactivation of LCCs. Next, we derive the associated ODEs for the moments of these densities, and truncate and close the moment equations to produce reduced models that faithfully reproduce Markov chain and population density results. Using both the population density and moment-based models, we investigate the voltage-dependence of Ca^{2+}-inactivation that may occur through local Ca^{2+} signaling in heterogeneous domains, and how Ca^{2+}-inactivation of L-type channels may be influenced by non-equilibrium dynamics of domain formation and collapse.

2 Model Formulation

The compartments and fluxes included in the model formulation are shown in Fig. 1 (right panel), which includes the [Ca^{2+}] in the extracellular space (c_{ext}), the cytosol (c_{cyt}), and the *nth* domain ($c^{(n)}$). For simplicity, we here assume that c_{ext} and c_{cyt} are clamped; however, it is straightforward to extend the model to account for the dynamics of c_{cyt} (see Sect. 4). Fluxes between compartments include the influx from the extracellular space to the *nth* individual domain ($J^{(n)}_{influx}$), and the flux from each domain to the cytoplasm ($J^{(n)}_{cyt}$).

Consistent with Fig. 1, the time-dependent dynamics of the [Ca^{2+}] in the *nth* domain is governed by the following ODE,

$$\frac{dc^{(n)}}{dt} = \frac{1}{\lambda_d}\left(\xi^i J^{(n)}_{influx} - J^{(n)}_{cyt}\right), \tag{1}$$

where $\xi^i = 0$ or 1 depending on whether the associated LCC is closed or open. Note that the superscript i indicates the channel's state and the superscript (n) represents the *nth* domain. In Eq. 1, $\lambda_d = (\Omega_d/\beta_d)/(\Omega_{cyt}/\beta_{cyt})$ is an effective volume ratio between the domain and cytoplasm, where Ω_d and Ω_{cyt} are the volumes of domain and cytoplasm, respectively, and β_d and β_{cyt} account for the buffering capacity of domain and cytoplasm. The flux from the domain to the cytoplasm is given by $J^{(n)}_{cyt} = v_{cyt}(c^{(n)} - c_{cyt})$, where v_{cyt} is the rate constant for Ca^{2+} domain collapse (units of time^{-1}). Note that Eq. 1 is linear and consequently, in case $\xi^i = 0$, $\tau = \lambda_d/v_{cyt}$ can be interpreted as the exponential time constant of domain collapse. A large value of τ indicates slow domains and a small τ indicates fast domains. The voltage- and Ca^{2+}-dependent influx, $J^{(n)}_{influx}$, is given by the Goldman-Hodgkin-Katz current equation (Hille 2001). That is, if the *nth* LCC is open, $J^{(n)}_{influx} = -A_m \imath^{(n)}_{influx}/(zF)$ where $A_m = C_m\beta_{cyt}/\Omega_{cyt}$ is a whole-cell capacitance scaling factor, C_m is the capacitive membrane area, $z = 2$ is the valence of Ca^{2+} and F is Faraday's constant. The Ca^{2+} current, $\imath^{(n)}_{influx}$, is given by $\imath^{(n)}_{influx} = z^2 FPV(c^{(n)} - c_{ext}e^{-zV/V_\theta})/[V_\theta(1 - e^{-zV/V_\theta})]$ where P is the permeability, V is the membrane voltage, $V_\theta = RT/F$, R is the gas constant, and T is the absolute temperature.

2.1 Twelve-state LCC Model

The LCC model used in this paper was introduced by Jafri et al. (1998) and reparameterized by Greenstein and Winslow (2002). The gating of the LCC is represented by a continuous-time, discrete-state Markov chain with twelve states, ten of which are non-conducting (closed) and two of which are conducting (open). As illustrated in Fig. 2, the upper and lower rows of states are Ca^{2+}-unbound (mode normal) and Ca^{2+}-bound (mode Ca), respectively. When in mode Ca, transitions to the open state O_{Ca} are extremely rare, because $g'_+ \ll g_+$. Transitions from mode normal to mode Ca depend on the rate constant $\gamma = \gamma_0 c^{(n)}$, which is a linear function

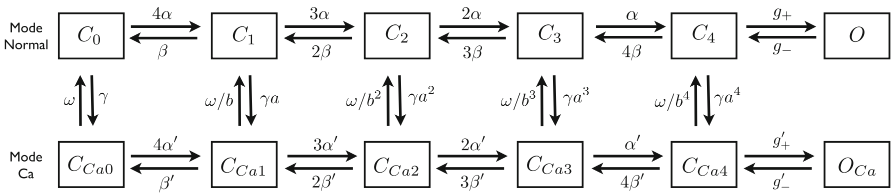

Fig. 2 Gating scheme of the L-type channel. The 12-state L-type Ca^{2+} channel includes Ca^{2+}-unbound and Ca^{2+}-bound states (denoted mode normal and mode Ca, respectively). In both modes there are *five closed states* ($C_0, \ldots, C_4$ and $C_{Ca0}, \ldots, C_{Ca4}$) and *one open state* (O and O_{Ca}). Transitions from mode normal to mode Ca depend on the rate constants γ (proportional to domain $[Ca^{2+}]$) and ω. Voltage-dependent transitions are determined by rates $\alpha(V)$ and $\beta(V)$ (mode normal) and $\alpha'(V)$ and $\beta'(V)$ (mode Ca). Parameters follow Greenstein and Winslow (2002), $\alpha = \alpha_0 \exp(\alpha_1(V - V_0))$, $\beta = \beta_0 \exp(\beta_1(V - V_0))$, $\alpha' = a\alpha$, $\beta' = \beta/b$, $\gamma = \gamma_0 c^{(n)}$, $g_+ = 0.85\,\text{ms}^{-1}$, $g_- = 2\,\text{ms}^{-1}$, $g'_+ = 0.005\,\text{ms}^{-1}$, $g'_- = 7\,\text{ms}^{-1}$, $\alpha_0 = 2.0$, $\alpha_1 = 0.0012$, $\beta_0 = 0.0882$, $\beta_1 = -0.05$, $a = 2$, $b = 1.9356$, $\gamma_0 = 0.44\,\text{mM}^{-1}\,\text{ms}^{-1}$, $\omega = 0.01258\,\text{ms}^{-1}$ and $V_0 = 35\,\text{mV}$

of the domain $[Ca^{2+}]$, that is, high $[Ca^{2+}]$ induces more transitions to mode Ca (more Ca^{2+}-dependent inactivation). In both mode normal and mode Ca, there are five closed states ($C_0, \ldots, C_4$ and $C_{Ca0}, \ldots, C_{Ca4}$) and one open state (O and O_{Ca}). Voltage-dependent transitions are determined by rate constants $\alpha(V)$ and $\beta(V)$, which are increasing and decreasing functions of membrane voltage, respectively (see Fig. 2, caption). We assume that each domain includes a single L-type Ca^{2+} channel. In the Markov chain model, the SSA method (Gillespie 1976) is utilized to simulate the dynamics of stochastic gating.

The transition rates between the 12 states of the LCC model can be written as a 12 × 12 infinitesimal generator matrix (Q matrix) that takes the form

$$Q(V, c) = K_\phi(V) + cK_c, \tag{2}$$

where for clarity we have dropped the superscripted index (n) and write c rather than $c^{(n)}$ for domain $[Ca^{2+}]$. In this expression, $K_\phi(V)$ collects the Ca^{2+}-independent transitions (both voltage-dependent and voltage-independent with units of time^{-1}), K_c includes the bimolecular association rate constants (units of $\text{time}^{-1}\,\text{concentration}^{-1}$) for the transitions mediated by domain Ca^{2+}. $K_\phi(V)$ and K_c are 12 × 12 matrices consistent with the transition-state diagram (Fig. 2):

$$\begin{array}{ccccc}
[K_\phi]_{1,2} = 4\alpha & [K_\phi]_{2,3} = 3\alpha & [K_\phi]_{3,4} = 2\alpha & [K_\phi]_{4,5} = \alpha & [K_\phi]_{5,6} = g_+ \\
[K_\phi]_{2,1} = \beta & [K_\phi]_{3,2} = 2\beta & [K_\phi]_{4,3} = 3\beta & [K_\phi]_{5,4} = 4\beta & [K_\phi]_{6,5} = g_- \\
[K_\phi]_{7,8} = 4\alpha' & [K_\phi]_{8,9} = 3\alpha' & [K_\phi]_{9,10} = 2\alpha' & [K_\phi]_{10,11} = \alpha' & [K_\phi]_{11,12} = g'_+ \\
[K_\phi]_{8,7} = \beta' & [K_\phi]_{9,8} = 2\beta' & [K_\phi]_{10,9} = 3\beta' & [K_\phi]_{11,10} = 4\beta' & [K_\phi]_{12,11} = g'_- \\
[K_\phi]_{7,1} = \omega & [K_\phi]_{8,2} = \omega/b & [K_\phi]_{9,3} = \omega/b^2 & [K_\phi]_{10,4} = \omega/b^3 & [K_\phi]_{11,5} = \omega/b^4 \\
[K_c]_{1,7} = \gamma_0 & [K_c]_{2,8} = \gamma_0 a & [K_c]_{3,9} = \gamma_0 a^2 & [K_c]_{4,10} = \gamma_0 a^3 & [K_c]_{5,11} = \gamma_0 a^4.
\end{array}$$

The diagonal elements of K_ϕ and K_c are such that each row sums to zero, i.e., $[K_\phi]_{ii} = -\sum_{j \neq i} [K_\phi]_{ij}$ and $[K_c]_{ii} = -\sum_{j \neq i} [K_c]_{ij}$, where $i = 1, 2, \ldots, 12$.

2.2 Population Density Formulation

The population density approach to modeling the domain Ca^{2+}-mediated inactivation of L-type Ca^{2+} channels is an alternative approach of the Markov chain model. Assuming a large number (N) of domains, we define a continuous univariate probability density function for the domain $[\mathrm{Ca}^{2+}]$ of a randomly sampled channel,

$$\rho^i(c,t)\,dc = \Pr\{c < \tilde{c}(t) < c + dc \quad \text{and} \quad \tilde{S}(t) = i\}, \tag{3}$$

where the index $i \in \{C_0, C_1, \ldots, O_{Ca}\}$ runs over the twelve states of the LCC, and the tildes on $\tilde{c}(t)$ and $\tilde{S}(t)$ indicate random quantities. The time-evolution of these joint probability densities is governed by the following system of advection-reaction equations (Bertram and Sherman 1998; Mazzag et al. 2005; Williams et al. 2007; Huertas and Smith 2007),

$$\frac{\partial \rho^i}{\partial t} = -\frac{\partial}{\partial c}[f^i \rho^i] + [\boldsymbol{\rho} Q]^i, \tag{4}$$

where i is an index over channel states, Q is the generator matrix given by Eq. 2, the row vector $\boldsymbol{\rho} = (\rho^{C_0},\ \rho^{C_1}, \ldots,\ \rho^{O_{Ca}})$ collects the time-dependent joint probability densities for domain $[\mathrm{Ca}^{2+}]$, and $[\boldsymbol{\rho} Q]^i$ is the *ith* element of the vector-matrix product $\boldsymbol{\rho} Q$. In Eq. 4, the reaction terms $[\boldsymbol{\rho} Q]^i$ account for the probability flux associated with channel state changes. The advection terms of the form $-\partial(f^i\rho^i)/\partial c$ represent the divergence of the probability flux $\phi^i(c,t) = f^i(c)\rho^i(c,t)$, where the advection rates $f^i(c)$ account for the state-dependent deterministic dynamics of domain $[\mathrm{Ca}^{2+}]$,

$$f^i = \frac{1}{\lambda_d^T}\left(\xi^i J_{influx} - J_{cyt}\right), \tag{5}$$

where $\lambda_d^T = N\lambda_d$. The aggregate flux from Ca^{2+} domains to cytosol is given by $J_{cyt} = v_{cyt}^T(c - c_{cyt})$, where $v_{cyt}^T = N v_{cyt}$ is the total rate of Ca^{2+} domain collapse and $\tau = \lambda_d^T / v_{cyt}^T$ is the domain time constant. The total influx term J_{influx} is linear in domain $[\mathrm{Ca}^{2+}]$ and can be written as $J_{influx} = \jmath_0 - \jmath_1 c$, where $\jmath_0 = zA_m P^T V c_{ext} e^{-zV/V_\theta} / [V_\theta(1 - e^{-zV/V_\theta})]$ and $\jmath_1 = zA_m P^T V / [V_\theta(1 - e^{-zV/V_\theta})]$, and where $P^T = NP$ is the total permeability. As mentioned before, the Ca^{2+} influx in each individual domain is linearly depedent on the influx current (i.e., $\jmath_{influx}^{(n)} = -A_m i_{influx}^{(n)}/(zF)$). Consequently, the whole cell Ca^{2+} current is given by

$$I_{influx} = \frac{zF}{A_m}\int(-\jmath_0 + \jmath_1 c)(\rho^O + \rho^{O_{Ca}})\,dc. \tag{6}$$

The time evolution of the joint densities $\rho^i(c,t)$, i.e., the dependent variables of the population density model, are found by integrating Eqs. 4–5 using a total variation diminishing scheme that has been described previously (Williams et al. 2007;

Huertas and Smith 2006). The most important observable of the model is the probability that a randomly sampled LCC is in a given state,

$$\Pr(\tilde{S}(t) = i) = \int \rho^i(c,t)\, dc, \tag{7}$$

where $i \in \{C_0, C_1, \ldots, O_{Ca}\}$. Another important observable is the expected [Ca^{2+}] in a randomly sampled domain,

$$E[\tilde{c}](t) = \sum_i \int c\rho^i(c,t)\, dc. \tag{8}$$

The expected [Ca^{2+}] conditioned on a randomly sampled channel being in state *i* is

$$E^i[\tilde{c}](t) = E[\tilde{c} \big| \tilde{S}(t) = i](t) = \frac{\int c\rho^i(c,t)\, dc}{\int \rho^i(c,t)\, dc}. \tag{9}$$

2.3 Moment-based LCC Model

The probability density approach described above is generally fast compared to the SSA simulation, in part because the joint densities are univariate. However, this computational advantage diminishes when an LCC model is complex, because one joint density is required for each state. In this section, we develop a moment-based modeling approach that is computationally more efficient than the population density approach.

We begin by writing the *qth* moment of the *ith* joint density as

$$\mu^i_q(t) = \int c^q \rho^i(c,t) dc. \tag{10}$$

This expression implies that the zeroth moments μ^i_0 are the time-dependent probabilities that a randomly sampled channel is in state *i* (Eq. 7). The first moments, $\mu^i_1(t) = \int c\rho^i dc$, are related to the expected value of domain [Ca^{2+}] conditioned on channel state: $\mathrm{E}^i[\tilde{c}] = \mu^i_1/\mu^i_0$ (cf. Eq. 9). The conditional variance in a randomly sampled domain is a function of the first three moments: $\mathrm{Var}^i[\tilde{c}] = \mu^i_2/\mu^i_0 - (\mu^i_1/\mu^i_0)^2$. The derivation of the moment-based LCC model begins by differentiating Eq. 10 with respect to time,

$$\frac{d\mu^i_q}{dt} = \int c^q \frac{\partial \rho^i}{\partial t}\, dc. \tag{11}$$

The ODEs of the moment-based model are found by replacing the factor $\partial\rho^i/\partial t$ in the integrand of Eq. 11 by the advection-reaction equation of the population density model (Eq. 4), which yields

$$
\begin{aligned}
\frac{d\mu_q^i}{dt} &= \int c^q \left[-\frac{\partial (f^i \rho^i)}{\partial c} + [\boldsymbol{\rho} Q]^i \right] dc \\
&= - \int c^q \, d(f^i \rho^i) + \int c^q \left[\boldsymbol{\rho} (K_\phi + c K_c) \right]^i dc.
\end{aligned}
$$

Integrating by parts gives

$$
\frac{d\mu_q^i}{dt} = q \int f^i c^{q-1} \rho^i dc + [\boldsymbol{\mu}_q K_\phi]^i + [\boldsymbol{\mu}_{q+1} K_c]^i, \tag{12}
$$

where we have eliminated terms using the fact that $\phi^i(c,t) = f^i(c)\rho^i(c,t) = 0$ on the boundary (conservation of probability). We evaluate the first integral of Eq. 12 by substituting Eq. 5 for f^i and simplifying,

$$
\begin{aligned}
q \int f^i c^{q-1} \rho^i dc &= q \int \left(\frac{\xi^i (\jmath_0 - \jmath_1 c)}{\lambda_d^T} - \frac{c - c_{cyt}}{\tau} \right) c^{q-1} \rho^i dc \\
&= q \left(\frac{\xi^i \jmath_0}{\lambda_d^T} + \frac{c_{cyt}}{\tau} \right) \mu_{q-1}^i - q \left(\frac{\xi^i \jmath_1}{\lambda_d^T} + \frac{1}{\tau} \right) \mu_q^i.
\end{aligned} \tag{13}
$$

Finally, substituting Eq. 13 into Eq. 12 results in the following equation for μ_q^i,

$$
\frac{d\mu_q^i}{dt} = q \left(\frac{\xi^i \jmath_0}{\lambda_d^T} + \frac{c_{cyt}}{\tau} \right) \mu_{q-1}^i - q \left(\frac{\xi^i \jmath_1}{\lambda_d^T} + \frac{1}{\tau} \right) \mu_q^i + [\boldsymbol{\mu}_q K_\phi]^i + [\boldsymbol{\mu}_{q+1} K_c]^i. \tag{14}
$$

where $\xi^i = 0$ for $i \in \{C_0, \ldots, C_4, C_{Ca0}, \ldots, C_{Ca4}\}$ and $\xi^i = 1$ for $i \in \{O, O_{Ca}\}$, $\boldsymbol{\mu}_q = (\mu_q^{C_0}, \ldots, \mu_q^{O_{Ca}})$, $\boldsymbol{\mu}_{q+1} = (\mu_{q+1}^{C_0}, \ldots, \mu_{q+1}^{O_{Ca}})$, and $[\boldsymbol{\mu}_q K_\phi(V)]^i$ and $[\boldsymbol{\mu}_{q+1} K_c]^i$ are the *ith* element of the vector-matrix product of $\boldsymbol{\mu}_q K_\phi(V)$ and $\boldsymbol{\mu}_{q+1} K_c$, respectively. Note that Eq. 14 is an open system of ODEs that takes the form

$$
\frac{d\mu_0^i}{dt} = \chi_0^i(\boldsymbol{\mu}_0, \boldsymbol{\mu}_1), \tag{15}
$$

$$
\frac{d\mu_q^i}{dt} = \chi_q^i(\boldsymbol{\mu}_{q-1}, \boldsymbol{\mu}_q, \boldsymbol{\mu}_{q+1}), \quad q = 1, 2, 3, \ldots \tag{16}
$$

In particular, note that the equations for the *qth* moments depend on the $(q+1)th$ moments.

2.4 Truncation and Closure of Moment ODEs

Equations 15–16 can be closed by assuming the $(q+1)th$ central moment (i.e., the moment about the mean) is zero, so that μ_{q+1}^i can be expressed as an algebraic function of lower moments. For example, the variance $\mathrm{Var}^i[\tilde{c}] = \mathrm{E}^i[(\tilde{c} - \mathrm{E}^i[\tilde{c}])^2] = \mu_2^i/\mu_0^i - \left(\mu_1^i/\mu_0^i\right)^2$ is the second central moment of the random variable $\tilde{c}$

conditioned on the channel being in state i. If we assume that the conditional variance is zero for each state i (i.e., $\mathrm{Var}^i[\tilde{c}] = 0$), the second moments are an algebraic function of the zeroth and first moments: $\mu_2^i = \left(\mu_1^i\right)^2/\mu_0^i$. In this case, Eqs. 15–16 can be truncated and closed as follows:

$$\frac{d\mu_0^i}{dt} = \chi_0^i(\boldsymbol{\mu}_0, \boldsymbol{\mu}_1), \tag{17}$$

$$\frac{d\mu_1^i}{dt} = \chi_1^i(\boldsymbol{\mu}_0, \boldsymbol{\mu}_1, \boldsymbol{\mu}_2(\boldsymbol{\mu}_0, \boldsymbol{\mu}_1)). \tag{18}$$

Closing the moment equations in this manner results in two ODEs per channel state—one for the zeroth moment μ_0^i, and the other one for the first moment μ_1^i (24 ODEs in total):

$$\frac{d\mu_0^i}{dt} = [\boldsymbol{\mu}_0 K_\phi]^i + [\boldsymbol{\mu}_1 K_c]^i \tag{19}$$

$$\frac{d\mu_1^i}{dt} = \left(\frac{\xi^i \jmath_0}{\lambda_d^T} + \frac{c_{cyt}}{\tau}\right)\mu_0^i - \left(\frac{\xi^i \jmath_1}{\lambda_d^T} + \frac{1}{\tau}\right)\mu_1^i + [\boldsymbol{\mu}_1 K_\phi]^i + [\boldsymbol{\mu}_2 K_c]^i, \tag{20}$$

where μ_2 is a row vector with elements $\mu_2^i = \left(\mu_1^i\right)^2/\mu_0^i$.

Alternatively, we assume the $3rd$ central moments to be zero. In that case, the truncated and closed moment equations take the form

$$\frac{d\mu_0^i}{dt} = \chi_0^i(\boldsymbol{\mu}_0, \boldsymbol{\mu}_1) \tag{21}$$

$$\frac{d\mu_1^i}{dt} = \chi_1^i(\boldsymbol{\mu}_0, \boldsymbol{\mu}_1, \boldsymbol{\mu}_2) \tag{22}$$

$$\frac{d\mu_2^i}{dt} = \chi_2^i(\boldsymbol{\mu}_1, \boldsymbol{\mu}_2, \boldsymbol{\mu}_3(\boldsymbol{\mu}_0, \boldsymbol{\mu}_1, \boldsymbol{\mu}_2)), \tag{23}$$

where

$$\mu_3^i = \frac{3\mu_2^i \mu_1^i}{\mu_0^i} - \frac{2(\mu_1^i)^3}{(\mu_0^i)^2}. \tag{24}$$

This assumption results in a moment-based model that includes 36 ODEs:

$$\frac{d\mu_0^i}{dt} = [\boldsymbol{\mu}_0 K_\phi]^i + [\boldsymbol{\mu}_1 K_c]^i \tag{25}$$

$$\frac{d\mu_1^i}{dt} = \left(\frac{\xi^i \jmath_0}{\lambda_d^T} + \frac{c_{cyt}}{\tau}\right)\mu_0^i - \left(\frac{\xi^i \jmath_1}{\lambda_d^T} + \frac{1}{\tau}\right)\mu_1^i + [\boldsymbol{\mu}_1 K_\phi]^i + [\boldsymbol{\mu}_2 K_c]^i \tag{26}$$

$$\frac{d\mu_2^i}{dt} = 2\left(\frac{\xi^i \jmath_0}{\lambda_d^T} + \frac{c_{cyt}}{\tau}\right)\mu_1^i - 2\left(\frac{\xi^i \jmath_1}{\lambda_d^T} + \frac{1}{\tau}\right)\mu_2^i + [\boldsymbol{\mu}_2 K_\phi]^i + [\boldsymbol{\mu}_3 K_c]^i \tag{27}$$

where μ_3 is a row vector with elements $\mu_3^i = 3\mu_2^i\mu_1^i/\mu_0^i - 2(\mu_1^i)^3/(\mu_0^i)^2$.

Below, Eqs. 25–27 are referred to as the "third-order moment truncation approach" while Eqs. 19–20 are called the "second-order moment truncation approach."

3 Results

3.1 Representative Population Density Simulation Results

To illustrate the population density approach to modeling domain Ca^{2+}-mediated inactivation, we first show simulations of a two-pulse voltage clamp protocol, analogous to those used in the experimental quantification of Ca^{2+}-inactivation of LCCs (Sherman et al. 1990; Plant 1988). As shown in the top panel of Fig. 3a, the simulated command voltage began at the holding potential of $V_h = -50\,\text{mV}$, and the joint densities of the model equations were equilibrated with this voltage. The command voltage was then stepped up to various prepulse potentials, V_p, and held at V_p for a prescribed length of time, t_p. The voltage was then stepped back down to the holding potential, V_h, for duration t_h, and then up to the test potential given by V_t. Channel inactivation was measured by estimating the inactivation function,

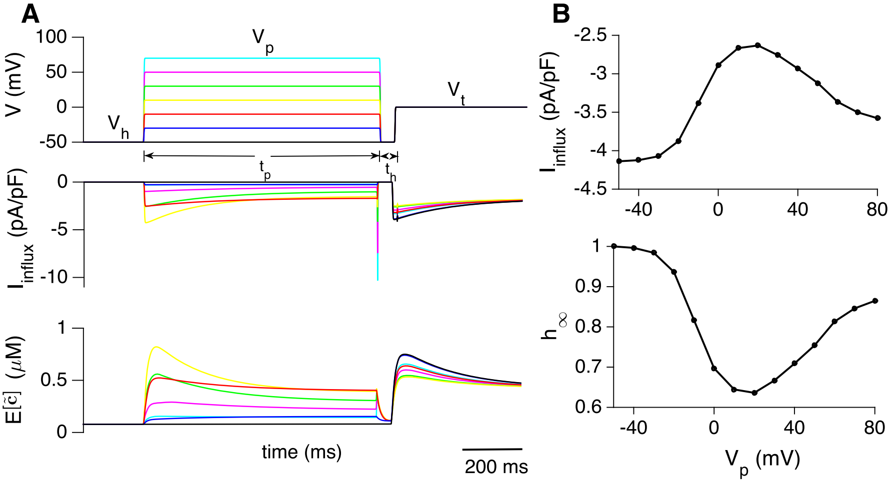

Fig. 3 Representative simulation results. **a** The response of the whole cell current (*middle panel*) and expected $[Ca^{2+}]$ (*bottom panel*) to the two-pulse voltage clamp protocol (*top panel*). **b** The peak current (*top panel*) and the inactivation function (Eq. 28, *bottom panel*) to a range of prepulse potentials ($-50 \le V_p \le 80\,\text{mV}$). Parameters: $V_h = -50\,\text{mV}, V_t = 0\,\text{mV}$, $V_p = -50$ to 80 mV, $t_p = 800\,\text{ms}$, $t_h = 50\,\text{ms}$, $\tau = 10\,\text{ms}$, and as in Fig. 2 and Table 1

Table 1 Parameters for the population density and moment-based model

Symbols	Definition	Units	Value
F	Faraday's constant	coul mol^{-1}	96,487
R	Gas constant	mJ mol^{-1}K^{-1}	8314
T	Absolute temperature	K	310
V_θ	RT/F	mV	26.72
P^T	Total permeability/specific capacitance	cm^{3}s^{-1} μF^{-1}	10^{-4}
C_m	Capacitance	μF	1.534×10^{-4}
A_m	Capacitive to volume ratio	mF L^{-1}	356.7
λ_d^T	Effective volume ratio of domain and cytosol	–	0.1
c_{ext}	Extracellular Ca^{2+} concentration	mM	2
c_{cyt}	Bulk Ca^{2+} concentration	μM	0.1
c_{ss}	Maximum Ca^{2+} concentration (Eq. 30)	μM	35

See Fig. 2 for the parameters of the 12-state L-type Ca^{2+} channel

$h_\infty(V_p)$, defined as the normalized peak current during the test voltage pulse as a function of the prepulse potential (Sherman et al. 1990),

$$h_\infty(V_p) = \frac{\mathrm{peak}[\mathrm{I}(\mathrm{V_p})]}{\mathrm{peak}[\mathrm{I}(\mathrm{V_p} = \mathrm{V_h})]}. \tag{28}$$

The inactivation function $h_\infty(V_p)$ gives the fraction of channels that are not inactivated, and takes a value between 0 and 1. When $h_\infty = 1$, none of the channels are inactivated; when $h_\infty = 0$, all of the channels are inactivated.

The middle and bottom panel of Fig. 3a show the whole cell Ca^{2+} current (I_{influx}) and the mean domain [Ca^{2+}] (E[$\tilde{c}$]) during the simulated two-pulse protocol. The largest inward currents during the test phase occurred when the prepulse voltage V_p was very low or very high (Fig. 3b top panel). This is consistent with the observation that during the prepulse phase little current was expressed at extreme voltages, preventing an accumulation of domain Ca^{2+} that could potentially inactivate LCCs. The spike current at the end of t_p is a tail current that is caused by the sudden increase in the driving force for the Ca^{2+} current when the command voltage is returned to the holding potential (Table 1).

The lower panel of Fig. 3b shows the inactivation curve $h_\infty(V_p)$ calculated via Eq. 28. Similar to the peak current, the inactivation function is biphasic with minimal Ca^{2+} inactivation ($h \approx 1$) when the repulse potential is very low or high, and maximum Ca^{2+} inactivation ($h \approx 0.65$) for intermediate repulse potentials. The shape of the inactivated curve is similar to the simulation result in Greenstein and Winslow (2002) and experimental results such as Ashcroft and Stanfield (1982).

Figure 4a shows the model response to the two-pulse voltage clamp protocol using a range of domain time constants (τ). Slower domain time constants (large τ, purple line) lead to decreased inward whole cell currents during the prepulse phase (compare green and red lines). This is consistent with the observation that a slow

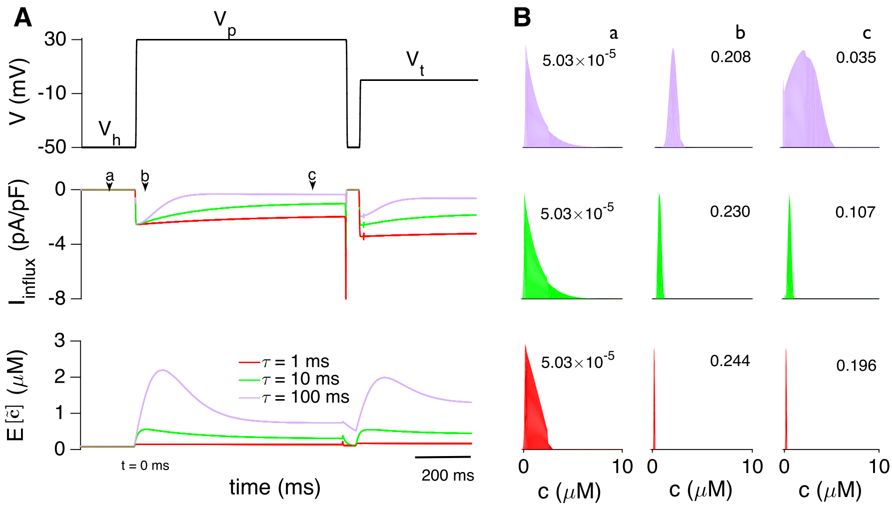

Fig. 4 **a** Command voltage traces, Ca^{2+} current and expected [Ca^{2+}] when domain time constant τ is varied. **b** Snapshot of the sum of the joint densities for open states, $\rho^O + \rho^{O_{Ca}}$, at three different times (*a*, *b*, *c*) and three domain time constants. Parameters: $\tau = 1\,\text{ms}$ (*red*), 10 ms (*green*) and 100 ms (*purple*), times *a*, *b* and *c* are shown as *arrows* at -100, 50 and 700 ms in (**a**), $V_h = -50\,\text{mV}$, $V_p = 30\,\text{mV}$, $V_t = 0\,\text{mV}$, and as in Fig. 2 and Table 1

domain time constant leads to higher expected domain [Ca^{2+}] and more Ca^{2+} inactivation.

Figure 4b shows the sum of the joint density functions of open states (i.e., $\rho^O + \rho^{O_{Ca}}$) for three different domain time constants at three different times during the two-pulse protocol (arrows labeled a, b, c in panel A). Note that these densities have been normalized for clarity, so the integrated areas no longer correspond to the probability that a channel is open. Consistent with Fig. 4a, this probability at time $t = 50$ ms (b) is higher than at times $t = -100$ and 700 ms (a and c, respectively), regardless of the domain time constant. When τ is small (fast domain), the density functions (red and green shaded regions) are narrow and δ-function-like (small variance). When τ is large (slow domain), the densities have greater variance (purple shaded regions).

3.2 Comparison of Population Density and Moment Closure Approaches

Figure 5 compares the moment-based model that uses second-order and third-order truncation methods to the corresponding population density and Markov chain model. The agreement between the Markov chain (○) and the population density (+ and ×) simulations validates our model. When τ is fast or intermediate (e.g., $\tau = 10$ ms), the assumption of zero variance (green) leads to nearly the same result as the population density model (+ symbols). However, when τ is slow (e.g., $\tau = 1$ s), the result computed from the second-order moment truncation approach (khaki) deviates slightly from the population density model (× symbols). As might be expected, this small error is eliminated using the third-order moment truncation

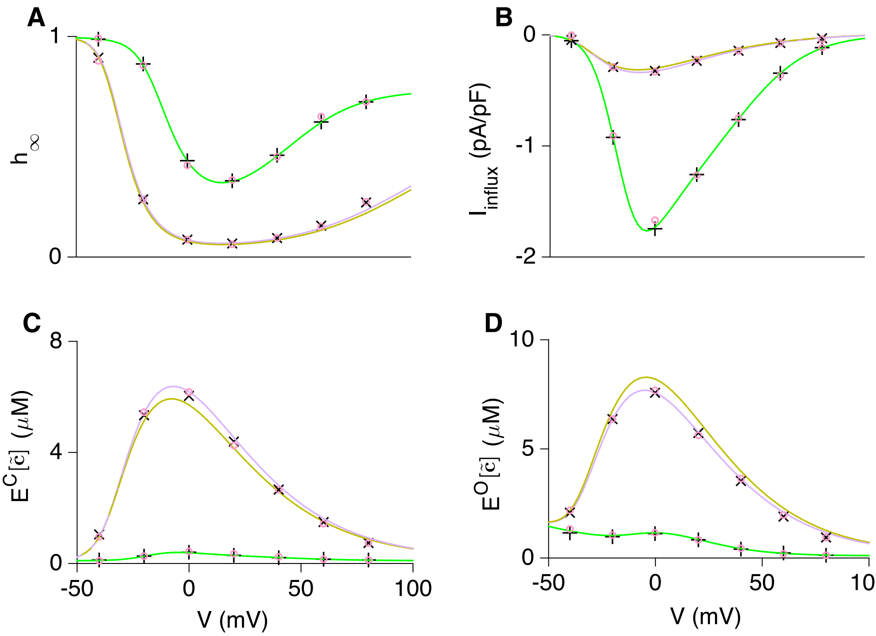

Fig. 5 Comparison between different moment closure techniques and the population density model. Steady-state Ca^{2+}-inactivation function (h_∞, **a**), total influx current (I_{influx}, **b**), expected $[Ca^{2+}]$ at *closed state* ($E^C[\tilde{c}]$, **c**) and *open state* ($E^O[\tilde{c}]$, **d**) as a function of voltage (V). *Green* and *khaki lines* are calculated via the second-order moment-based LCC model when $\tau = 10$ ms and 1 s, respectively. The *purple line* is calculated via the third-order moment-based model when τ is 1 s. *Plus* and *times* symbols are computed via the population density model when τ is 10 ms and 1 s respectively. *Open circles* symbols are computed using the corresponding Markov chain model, assuming the number of L-type Ca^{2+} channels is 200. Other parameters as in Fig. 2 and Table 1

approach (purple). Moment-based calculations in the remainder of the paper will utilize the third-order truncation method, which accurately approximate the population density model for domain time constants in the physiological range ($\tau = 0.1$ ms to 1 s).

In general, the runtime of the population density model is fast when τ is large and slow when τ is small. However, even when $\tau = 1$ s and $V = 0$ mV, the population density model takes 79 s on average to simulate a 2 s trail (10 trails in total), while the mean runtime for the third-order moment-based model is only 0.16 s. The simulation time of the Markov chain model depends on the number of Ca^{2+} domains (N). When N is 200, the average runtime is 936 s for 2 s simulation. The models are implemented via MATLAB and simulated on a Mac Pro. The processor is 2.4 GHz Intel Core i7, and the RAM is 8 GB 1600 MHz DDR3.

3.3 Steady-state Ca^{2+}-inactivation and the Domain Time Constant

When an LCC is open, the time-dependence of domain $[Ca^{2+}]$ can be rewritten as

$$\frac{dc}{dt} = \frac{1}{\lambda_d^T}(\jmath_0 - \jmath_1 c) - \frac{c - c_{cyt}}{\tau}, \tag{29}$$

where $\jmath_0$ and $\jmath_1$ are defined above. From Eq. 29, it is straightforward to derive the steady state domain [Ca^{2+}] for an open LCC,

$$c_{ss} = \frac{\jmath_0/\lambda_d^T + c_{cyt}/\tau}{\jmath_1/\lambda_d^T + 1/\tau}. \tag{30}$$

The concentration c_{ss} is the maximum [Ca^{2+}] that can be achieved in a domain, its value depends on membrane voltage V, the domain time constant τ and the total permeability P^T, where V and P^T occur as parameters in $\jmath_0$ and $\jmath_1$. In this section we investigate how the domain time constant influences steady-state Ca^{2+}-inactivation under the assumption of fixed total permeability. In the following section, we consider the related question of the domain time constant's impact on steady-state Ca^{2+} inactivation when LCC permeability is adjusted so that the steady-state domain [Ca^{2+}] (c_{ss}) is fixed.

Figure 6 shows how the domain time constant (τ) influences the voltage-dependence of the steady-state Ca^{2+}-dependent inactivation of LCCs in the population density and moment-based models. For each domain time constant and voltage, the steady-state fraction of LCCs in four lumped states are shown, namely,

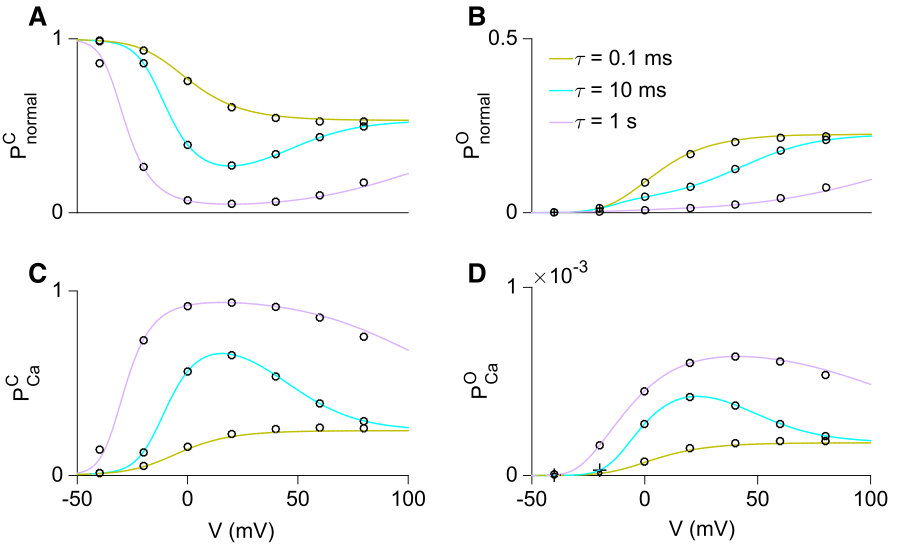

Fig. 6 Comparison of steady-state probabilities of L-type channel states when the domain time constant τ is varied. The fraction of channels in *closed states* of mode normal (P^C_{normal}, **a**) and mode Ca (P^C_{Ca}, **b**), and the fraction of channels in *open state* of mode normal (P^O_{normal}, **c**) and mode Ca (P^O_{Ca}, **d**), as a function of V_m. The *khaki*, *blue* and *purple lines* are the simulation results of the moment-based model when $\tau =$ 0.1 ms, 10 ms and 1 s, respectively. The corresponding population density simulation results are given by *open circles*. Parameters as in Fig. 2 and Table 1

mode normal open (P^O_{normal}), mode Ca open (P^O_{Ca}), mode normal closed (P^C_{normal}, including contributions from states $C_0, \ldots, C_4$), and mode Ca closed (P^C_{Ca}, states $C_{Ca0}, \ldots, C_{Ca_4}$). For all domain time constants studied, increasing the voltage leads to increased steady-state open probabilities ($P^O_{normal} + P^O_{Ca}$). Slowing the domain time constant increases the probability that a randomly sampled channel is in mode Ca ($P^C_{Ca} + P^O_{Ca}$), regardless of voltage and consistent with our prior observation that slower domain time constants result in higher domain [Ca^{2+}] (Fig. 4a) and a decreased probability for a channel to be open ($P^O_{normal} + P^O_{Ca}$). Note that the four plots are in different scales, however, the sum of probabilities in different states should add up to one.

Figure 7a shows the inactivation function (h_∞) at steady state when τ is varied from 0.1 ms to 1 s. As the domain time constant τ increases, the inactivation function shifts downwards, corresponding to increased Ca^{2+} channel inactivation. This results from residual Ca^{2+} lingering in the domain, increasing the expected [Ca^{2+}] (Fig. 7c). Although the expected domain [Ca^{2+}] increases with τ, the total Ca^{2+} current decreases (Fig. 7b) due to a decreased probability for a channel to be open. Figure 7d shows that the domain Ca^{2+} concentrations are more heterogeneous (higher variance) with slow domain collapse time, regardless of voltage. This is consistent with Fig. 4 where a small τ results in a narrow distribution and low variance and a large τ yields a broader distribution and higher variance.

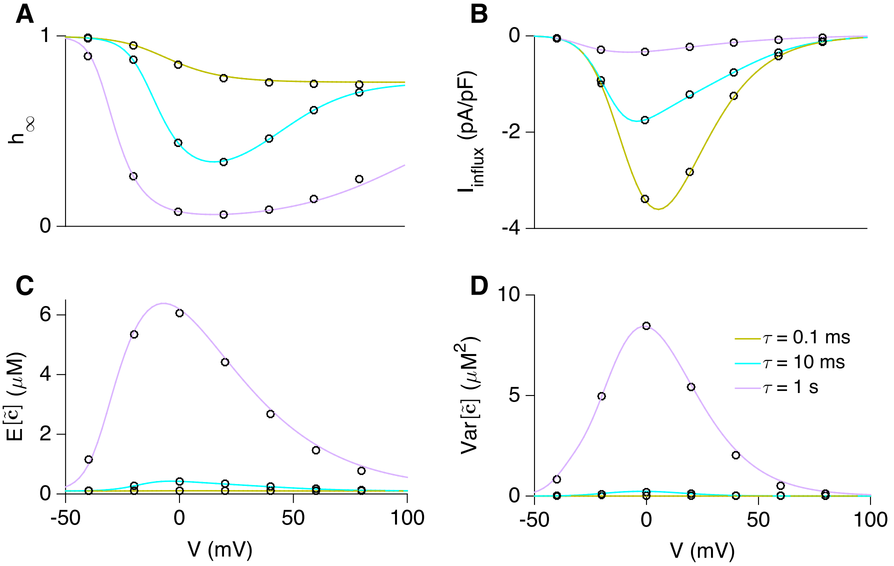

Fig. 7 Steady-state Ca^{2+}-inactivation and domain time constant τ with fixed P^T. Ca^{2+}-inactivation function (h_∞, A), Ca^{2+} influx current (I_{influx}, B), expected [Ca^{2+}] (E[$\tilde{c}$], C) and the variance of [Ca^{2+}] in different domains (Var[$\tilde{c}$], D) calculated via the moment-based model as a function of *V*. The corresponding population density simulation results are given by open circles. Parameters: $\tau = 0.1$ ms (*khaki*), 10 ms (*blue*) and 1 s (*purple*), and other parameters as in Fig. 2 and Table 1

3.4 Ca^{2+}-inactivation When Maximum [Ca^{2+}] is Fixed

In the parameter studies of Figs. 6 and 7, the permeability P^T was held constant as the domain time constant τ was varied. Structuring the parameter study in this manner allows τ to influence the domain dynamics by changing the rate of domain formation and collapse as well as the steady-state domain [Ca^{2+}], given by $c_{ss} = \left(\jmath_0/\lambda_d^T + c_{cyt}/\tau\right)/\left(\jmath_1/\lambda_d^T + 1/\tau\right)$. Figure 8 presents an alternative parameter study that controls for the effect of the domain time constant on the steady-state domain [Ca^{2+}], thereby highlighting the manner in which the rate of domain formation and collapse influences Ca^{2+}-mediated inactivation of LCCs.

Figure 8 shows that, for a given voltage and domain time constant τ, increasing the permeability of the channel (and thus c_{ss}, the maximum domain [Ca^{2+}] that can be achieved) leads to an increase in Ca^{2+}-mediated inactivation (decreased h_∞). On the other hand, when the permeability is adjusted so that the maximum domain [Ca^{2+}] is fixed, decreasing τ (faster domain) increases both the expected domain [Ca^{2+}] at open state (Fig. 8c) and Ca^{2+}-dependent inactivation (Fig. 8a). When c_{ss} is fixed, a slower domain leads to smaller variance, i.e., Ca^{2+} channels in different domains are likely to experience similar [Ca^{2+}] (Fig. 8d).

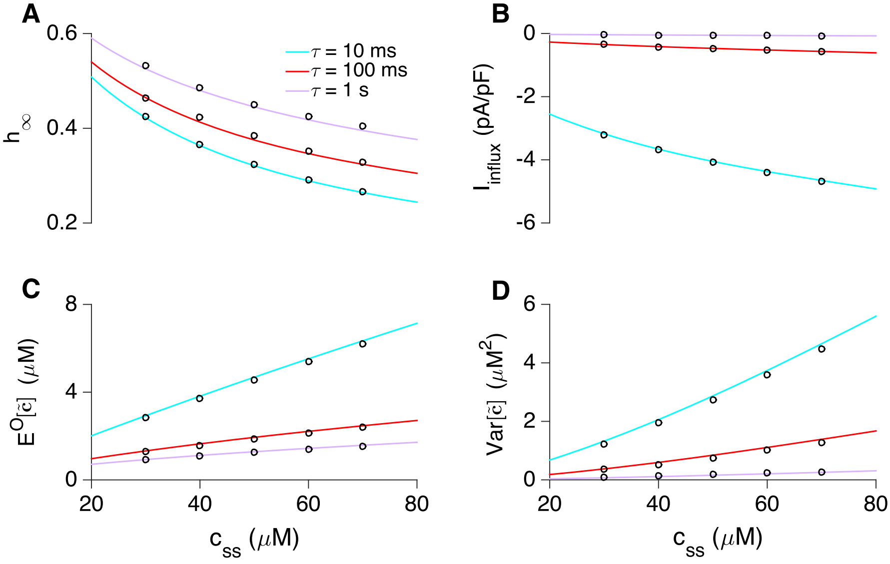

Fig. 8 Steady-state of Ca^{2+}-inactivation and domain time constant τ with c_{ss} and voltage fixed. h_∞, I_{influx}, $\mathrm{E}^{\mathrm{O}}[\tilde{c}]$ and $\mathrm{Var}[\tilde{c}]$ calculated via the moment-based model as a function of the maximum domain [Ca^{2+}], c_{ss}. The corresponding population density simulations are given by *open circles*. Parameters: $\tau = 10$ ms (*blue*), 100 ms (*red*) and 1 s (*purple line*), $V = -10\,\mathrm{mV}$, and others as Fig. 2 and Table 1

4 Conclusions and Discussion

4.1 Summary of Results

In this paper, we have shown how a population density approach (Eq. 4) to modeling Ca^{2+}-mediated inactivation of L-type Ca^{2+} channels is an extension of (and improvement upon) biophysical theory that assumes that domain $[Ca^{2+}]$ is proportional to single channel current (recall Fig. 1). The population density approach is similar to traditional domain models of Ca^{2+}-mediated inactivation (Sherman et al. 1990) in that both assume a large number of low-density Ca^{2+} channels and a minimally represent action of the heterogeneity of domain $[Ca^{2+}]$—a potentially important feature of Ca^{2+}-mediated inactivation that is not captured by common pool models.

However, the population density approach is distinct from traditional multiscale models of Ca^{2+}-inactivation in its representation of the time-dependent formation and collapse of Ca^{2+} domains associated with L-type channels. Similar to previous work focused on local control of excitation-contraction coupling in cardiac myocytes (Williams et al. 2007), the population density approach to modeling Ca^{2+} inactivation of L-type channels is often preferable to the SSA simulation of the stochastic dynamics of channels and domains. This is due to the fact that the computational efficiency of a population density model scales with the number of states in the Markov chain model of the L-type channel, as opposed to the (far greater) number of channels present in the plasma membrane of the cell. Traditional equilibrium domain models also have this advantage, but do not account for the dynamics of domain formation and collapse that may in some cases influence the kinetics of Ca^{2+} inactivation (Mazzag et al. 2005; Bertram and Sherman 1998).

The population density formalism allows the derivation of moment-based models of domain Ca^{2+} inactivation that are extremely computationally efficient. We have derived two different moment-based models that are distinguished by the number of ODEs per channel state retained after truncation of the open system of moment equations as well as by the assumptions made to close the moment equations. Both the second-order (Eqs. 19–20, zero variance) and third-order (Eqs. 25–27, zero third central moment) moment-based models performed well when validated by comparison to corresponding population density simulations, but the third-order moment-based model was extremely accurate and valid for a wider range of domain time constants (Fig. 5). The second-order moment-based model is most accurate when the domain time constant is relatively small (fast domain, $\tau \leq 10\,\mathrm{ms}$), because in that case the joint distributions for domain $[Ca^{2+}]$ conditioned on channel state are very focused (low variance, recall Fig. 5).

Using both the population density and moment-based models, we investigated the dependence of the steady-state inactivation of the 12-state L-type Ca^{2+} channel model (Greenstein and Winslow 2002) on the exponential time constant (τ) for domain formation and collapse. When the study was performed using a fixed permeability for the L-type channel, faster domains (smaller τ) lead to less inactivation for a wide range of clamped voltages. When the channel permeability is chosen to be a function of τ that results in a fixed maximum domain [Ca^{2+}], a smaller domain time constant leads to increased Ca^{2+}-mediated inactivation, presumably because the kinetics of domain formation subsequent to channel opening are more rapid. Similar results are obtained by implementing a four-state model (Sherman et al. 1990) via the population density and moment-based models (not shown).

4.2 Limitations and Possible Extensions

Although the computational efficiency of the probability density and moment-based calculations is notable, the runtimes of both models are proportional to the number of states in a given L-type channel model. Consequently, both methods may have little computational advantage if the LCC model of interest is extremely complex. In addition, the efficiency of the probability density approach is dependent upon the number of meshpoints used in solving the advection-reaction equations.

For simplicity, we have illustrated the population density and moment-based models under the assumption that plasma membrane fluxes do not change the bulk cytosolic [Ca^{2+}] (that is, c_{cyt} is clamped). However, it is straightforward to relax this assumption and thereby allow a dynamic bulk intercellular [Ca^{2+}]. For example, assuming the rate of ATP-dependent plasma membrane Ca^{2+}-efflux is given by $J_{out} = k_{out}\, c_{cyt}$, the ODE for bulk cytosolic Ca^{2+} is

$$\frac{dc_{cyt}}{dt} = J^*_{cyt} - J_{out}, \tag{31}$$

where J^*_{cyt} is the total flux from domains to cytosol,

$$\begin{aligned} J^*_{\text{cyt}}(t) =& \sum_i \int J_{cyt}\, \rho^i(c,t)\, dc \\ =& v^T_{cyt} \sum_i \int \left[c - c_{cyt}(t)\right] \rho^i(c,t)\, dc \\ =& v^T_{cyt} \left[\sum_i \mu^i_1 - c_{cyt}(t) \right]. \end{aligned}$$

In spite of the fact that we have chosen to illustrate the population density and moment-based models through simulated voltage clamp recordings, the modeling formalism is easily modified to simulate current clamp recordings. However, the modeling of the current clamp experiment might be harder due to the complex interaction between different channel types.

The 12-state LCC model used in this paper does not account for voltage-dependent inactivation. However, it is straightforward to implement LCC models that include both voltage-dependent activation/inactivation and Ca^{2+}-dependent inactivation. Moreover, the population density approach presented here is well-suited to investigate whole-cell potassium currents that arise through voltage- and

Ca^{2+}-dependent stochastic gating of small potassium (SK) and big potassium (BK) channels, both of which play important physiological roles in the heart, brain and muscle cells and are often spatially co-localized with L-type Ca^{2+} channels (Vandael et al. 2010; Vergaraa et al. 1988; Qi et al. 2014; Hammond et al. 2006; Pribnow et al. 1999). Previous work by Stanley et al. (2011) has shown that the stochastic gating of Ca^{2+} channels increases the activation of SK channels. Cox recently presented a $Ca_v\,2.1/BK_{Ca}$ model which suggested that Ca^{2+} channels will open during a typical cortical neuron action potential, while the associated BK_{Ca} channel opens in only $30\,\%$ of trials (Cox 2014). Furthermore, this percentage is sensitive to the action potential duration, the distance between the two channels in the signaling complex, and the concentration of intercellular Ca^{2+} buffers (Cox 2014). Extensions of the population density and moment-based model that account for the dynamic of Ca^{2+} buffering and the geometric relationship between channels is an important avenue for future research.

Acknowledgments The work was supported in part by National Science Foundation Grant DMS 1121606 to GDS and the Biomathematics Initiative at The College of William & Mary.

References

Ashcroft FM, Stanfield PR (1982) Calcium inactivation in skeletal muscle fibres of the stick insect, carausius morosus. J Physiol 330:349–372

Baumann L, Gerstner A, Zong X, Biel M, Wahl-Schott C (2004) Functional characterization of L-type Ca^{2+} channel $Ca_v1.4\alpha1$ from mouse retina. Invest Ophthal Vis Sci 45(2):708–713

Bers DM (2002) Cardiac excitation-contraction coupling. Nature 415(6868):198–205

Bertram R, Sherman A (1998) Population dynamics of synaptic release sites. SIAM J Appl Math 58(1):142–169

Budde T, Meuth S, Pape HC (2002) Calcium-dependent inactivation of neuronal calcium channels. Nat Rev Neurosci 3:873–883

Cannell MB, Cheng H, Lederer WJ (1995) The control of calcium release in heart muscle. Science 268(5213):1045–1049

Cheng H, Lederer WJ, Cannell MB (1993) Calcium sparks: elementary events underlying excitation-contraction coupling in heart muscle. Science 262(5134):740–744

Christel C, Lee A (2012) Ca^{2+}-dependent modulation of voltage-gated Ca^{2+} channel. Biochimica et Biophysica Acta (BBA)—General Subjects 1820(8):1243–1252

Cox DH (2014) Modeling a Ca^{2+} channel/BK_{Ca} channel complex at the single-complex level. Biophys J 107:2797–2814

Ertel EA, Campbell KP, Harpold MM, Hofmann F, Mori Y, Perez-Reyes E, Schwartz A, Snutch TP, Tanabe T, Birnbaumer L et al (2000) Nomenclature of voltage-gated calcium channels. Neuron 25(3):533–535

Gillespie DT (1976) A general method for numerically simulating the stochastic time evolution of coupled chemical reactions. J Comput Phys 22:403–434

Greenstein JL, Winslow RL (2002) An integrative model of the cardiac ventricular myocyte incorporating local control of Ca^{2+} release. Biophys J 83(6):2918–2945

Haack JA, Rosenberg RL (1994) Calcium-dependent inactivation of L-type calcium channels in planar lipid bilayers. Biophys J 66(4):1051–1060

Hammond RS, Bond CT, Strassmaier T, Ngo-Anh TJ, Adelman JP, Maylie J, Stackman RW (2006) Small-conductance Ca^{2+}-activated potassium channel type 2 (SK2) modulates hippocampal learning, memory, and synaptic plasticity. J Neurosci 26(6):1844–1853

Hartman JA, Sobie EA, Smith GD (2010) Calcium sparks and homeostasis in a minimal model of local and global calcium responses in quiescent ventricular myocytes. Am J Physiol Heart Cir Physiol 299: H1996–H2008 First published Spetember 17, 2010; doi: 10.1152/ajpheart.00293.2010

Hille B (2001) Ion channels of excitable membranes, 3rd edn. Sinauer Associates, Sunderland

Huang G, Kim JY, Dehoff M, Mizuno Y, Kamm KE, Worley PF, Muallem S, Zeng WZ (2014) Ca^{2+} signaling in microdomains: Homer1 mediates the interaction between RyR2 and $Ca_v1.2$ to regulate excitation-contraction coupling. J Biol Chem 282(19):14283–14290

Huertas MA, Smith GD (2006) A multivariate population density model of the dLGN/PGN relay. J Comput Neurosci 21(2):171–189

Huertas MA, Smith GD (2007) The dynamics of luminal depletion and the stochastic gating of Ca^{2+}-activated Ca^{2+} channels and release sites. J Theor Biol 246(2):332–354

Jafri MS, Rice JJ, Winslow RL (1998) Cardiac Ca^{2+} dynamics: the roles of ryanodine receptor adaptation and sarcoplasmic reticulum load. Biophys J 74(3):1149–1168

Koschak A, Reimer D, Huber I, Grabner M, Glossmann H, Engel J, Strissnig J (2001) α1D ($Ca_v1.3$) subunits can form L-type Ca^{2+} channels activating at negative voltages. J Biol Chem 276:22100–22106

Li YX, Rinzel J, Vergara L, Stojilković SS (1995) Spontaneous electrical and Ca^{2+} oscillations in unstimulated pituitary gonadotrophs. Biophys J 69(3):785–795

Lipscombe D, Helton TD, Xu W (2004) L-type calcium channels: the low down. J Neurophysiol 92:2633–2641

Lipscombe D, Pan QJ, Gray AC (2002) Functional diversity in neuronal voltage-gated Ca^{2+} channels by alternative splicing of $Ca_v\alpha_1$. Mol Neurobiol 26(1):21–44

Marcantoni A, Baldelli P, Hernandez-Guijo JM, Comunanza V, Carabelli V, Carbone E (2007) L-type calcium channels in adrenal chromatin cells: role in pace-making and secretion. Cell Calcium 42:397–408

Mazzag B, Tignanelli C, Smith GD (2005) The effect of residual Ca^{2+} on the stochastic gating of Ca^{2+}-regulated Ca^{2+} channels. J Theor Biol 235(1):121–150

Murphy TH, Vorley PF, Baraban JM (1991) L-type voltage-sensitive calcium channels mediate synaptic activation of immediate early genes. Neuron 7(4):625–635

Plant TD (1988) Properties and calcium-dependent inactivation of calcium currents in cultured mouse pancreatic B-cells. J Physiol 404:731–747

Pribnow D, Johnson-Pais T, Bond CT, Keen J, Johnson RA, Janowsky A, Silvia C, Thayer M, Maylie J, Adelman JP (1999) Skeletal muscle and small-conductance calcium-activated potassium channels. Muscle Nerve 22(6):742–750

Qi XY, Diness JG, Brundel BJ, Zhou XB, Naud P, Wu CT, Huang J, Harada M, Aflaki M, Dobrev D, Grunnet M, Nattel S (2014) Role of small-conductance calcium-activated potassium channels in atrial electrophysiology and fibrillation in the dog. Circulation 129(4):430–440

Sherman A, Keizer J, Rinzel J (1990) Domain model for Ca^{2+}-inactivation of Ca^{2+} channels at low channel density. Biophys J 58(4):985–995

Simon M, Perrier JF, Jounsgaard J (2003) Subcellular distribution of L-type Ca^{2+} channels responsible for plateau potentials in motoneurons from the lumbar spinal cord of the turtle. Eur J Neurosci 18:258–266

Stanley DA, Bardakjian BL, Spano ML, Ditto WL (2011) Stochastic amplification of Ca^{2+}-activated potassium currents in Ca^{2+} microdomains. J Comput Neurosci 31(3):647–666

Tanskanen AJ, Greenstein JL, O'Rouke B, Winslow RL (2005) The role of stochastic and modal gating of cardiac L-type Ca^{2+} channels on early after-depolarizations. Biophys J 88:85–95

Torrente A, Mesirca P, Neco P (2011) $Ca_v1.3$ L-type calcium channels-mediated ryanodine receptor dependent calcium release controls heart rate. Biophys J 100:567a

Vandael DH, Marcantoni A, Mahapatra S, Caro A, Ruth P, Zuccotti A, Knipper M, Carbone E (2010) $Ca_v1.3$ and BK channels for timing and regulating cell firing. Mol Neurobiol 42:185–198

Vergaraa C, Latorrea R, Marrionb NV, Adelmanb JP (1988) Calcium-activated potassium channels. Curr Opin Neurobiol 8(3):321–329

Williams GSB, Chikando AC, Tuan HT, Sobie EA, Lederer WJ, Jafri MS (2011) Dynamics of calcium sparks and calcium leak in the heart. Biophys J 101:1287–1296

Williams GSB, Huertas MA, Sobie EA, Jafri MS, Smith GD (2007) A probability density approach to modeling local control of Ca^{2+}-induced Ca^{2+} release in cardiac myocytes. Biophys J 92(7):2311–2328

Williams GSB, Huertas MA, Sobie EA, Jafri MS, Smith GD (2008) Moment closure for local control models of Ca^{2+}-induced Ca^{2+} release in cardiac myocytes. Biophys J 95(4):1689–1703

Zweifach A, Lewis RS (1995) Rapid inactivation of depletion-activated calcium current (ICRAC) due to local calcium feedback. J Gen Physiol 105(2):209–226